Statistical analysis for beam smoothing and some applications

J. Garnier

Centre de Mathématiques Appliquées, Unité de Recherche Associée au Centre National de la Recherche Scientifique 756, Ecole Polytechnique, 91128 Palaiseau Cedex, France

L. Videau and C. Gouédard

Commissariat à l'Energie Atomique, Centre d'Etudes de Limeil-Valenton, 94195 Villeneuve St. Georges Cedex, France

A. Migus

Commissariat à l'Energie Atomique, Centre d'Etudes de Limeil-Valenton, 94195 Villeneuve St. Georges Cedex, France, and Laboratoire pour l'Utilisation des Lasers Intenses, Unité Mixte de Recherche au Centre National de la Recherche Scientifique 100, Ecole Polytechnique, 91128 Palaiseau Cedex, France

Received July 8, 1996; revised manuscript received February 4, 1997; accepted February 12, 1997

We develop statistical tools for beam smoothing analysis. As applications we study the respective performances of two-dimensional smoothing by spectral dispersion and of smoothing by optical fiber. The calculations are valid in the asymptotic framework of a large number of elements of the random-phase plate and of excited optical modes of the fiber. Theoretical results and closed-form expressions for the contrast and the spatial spectrum of the integrated intensity of the speckle pattern are derived so as to produce evidence of performance differences between these methods, which are essentially based on the longer time delay induced by the multimode fiber with respect to that induced by the gratings and on the nature of the spectral broadening. [S0740-3232(97)02608-2]

1. INTRODUCTION

The implementation of smoothing techniques for uniform irradiation in plasma physics[1] has become an extensively studied object, especially in the light of the U.S. National Ignition Facility (NIF) project[2] and the French Laser MegaJoule (LMJ) project[3] for inertial confinement fusion. All active smoothing methods—induced spatial incoherence with echelons,[4] smoothing by spectral dispersion (SSD),[5] and smoothing by multimode optical fiber (SOF)[6]—involve illumination on the target with an intensity that is a time-varying speckle pattern, so that the time-integrated intensity averages toward a flat profile. The corresponding time-varying speckle pattern relies on the same general concept. First, a broadband pulse is generated either by a naturally incoherent broad source or by a frequency-modulated laser beam with the use of phase modulators. In the next step this broadband source is spatially dispersed and spatial random modulations are imposed on the spectral components to produce on target a moving speckle pattern, with Gaussian statistics for the electric field.

However, it should be emphasized that if the principles are unique, the values of the characteristic parameters of each method may differ by as much as 1 or 2 orders of magnitude. This is particularly true for the time delay induced by the dispersion of the frequencies across the beam, which is created by the gratings in the SSD implementation or by a multimode fiber in the SOF implementation. This should imply quite different smoothing properties. In particular, the distribution of the smoothed spatial frequencies will depend strongly on the selected method.

These general considerations lead to the need to develop statistical tools to determine the important characteristics of the smoothed beams. One approach, based on numerical simulations, has already been used to compare SSD and echelon-free induced spatial incoherence.[2] Our goal here is to develop a statistical analysis of beam smoothing that leads to closed-form expressions of the contrasts and the power spectral densities of the smoothed fluence distributions in order to get general laws for statistical properties of smoothing techniques. Indeed, the smoothing techniques involve a large number of components, so it should be convenient to have precise expressions to optimize all parameters. The paper is organized as follows. In Section 2 we review the elementary concepts behind smoothing techniques, and Sections 3 and 4 are devoted to SSD and SOF. Finally, Section 5 discusses some advanced concepts of phase modulation and multiple-beam overlap.

2. SIMPLIFIED INTRODUCTION TO OPTICAL SMOOTHING

A. Principles

The principle of optical smoothing consists in generating a time-varying speckle pattern, whose coherence time is as short as possible. This implies that broadband long pulses are needed. The time-integrated intensity is then a sum of N independent patterns, where N is the ratio of the integration time to the coherence time of the light. As a consequence, the fluctuations of the integrated intensity average toward 0 (strong law of large numbers[7]). More exactly, the contrast (i.e., the ratio of the variance to the mean intensity) will be reduced by $\sqrt{N}$. The principle of SSD is the following.[2,5,8] A broadband source is spectrally dispersed onto a random-phase plate (RPP), which consists of square elements imposing randomly a phase shift of 0 or π. Each square element of the RPP is illuminated by a different frequency. The beamlets generated by the elements focus onto the target; they interfere and form a speckle pattern. The key point is that the phases of the beamlets will vary in time according to their respective illumination frequencies. As a result, the interference terms between the different beamlets will average to zero, so that the integrated intensity will approach the smooth sinc^2 envelope. However, if several of the elements of the RPP are illuminated by the same frequency, there will be residual correlations, and unsmoothed structure will exist in the integrated intensity. This will actually be the case in any realistic configuration.

In this section we focus our attention on one-dimensional SSD (1D SSD), whose standard implementation is shown in Fig. 1. An incident monochromatic beam with wavelength λ_0 is spectrally broadened by a sinusoidal phase modulator with frequency ν and depth β. The spectrum consisting of approximately 2β sidebands is dispersed onto the RPP by a grating that induces a lateral time delay T_d. Let us look at how separated points in the near field interfere and contribute to the generation of the speckle pattern. In the plane of the RPP, the incident beam splits into elementary beams with diameter $\Delta X \sim D/(2\beta\nu T_d)$, where D is the near-field beam aperture. Points of the RPP that are separated by less than ΔX are coherently illuminated. Two successive sideband beams are uncorrelated, but two sideband beams separated by $D/(\nu T_d)$ are coherent, since the modulation is sinusoidal. As a consequence, approximately 2β uncorrelated sidebands can be created. So we can expect an asymptotic contrast reduction equal to $\sqrt{2\beta}$. Two elements of the RPP separated by less than ΔX are coherently illuminated. The angle of the interference between two points separated by ΔX is given by $\Delta\theta = \Delta X/f$, where f is the lens focal length. Thus these points contribute to spatial frequency on the target, given by $\nu_x = \Delta\theta/\lambda_0 = \Delta X/(f\lambda_0)$. So the spatial frequencies on the target (in the dispersion direction) less than $\Delta X/(f\lambda_0) = D/(2\beta\nu T_d\lambda_0 f)$ are not smoothed. Neither are the spatial frequencies multiple of $D/(\nu T_d\lambda_0 f)$, owing to the pure sinusoidal phase modulation. In what follows we shall exhibit closed-form expressions that will appear consistent with the heuristical arguments developed above.

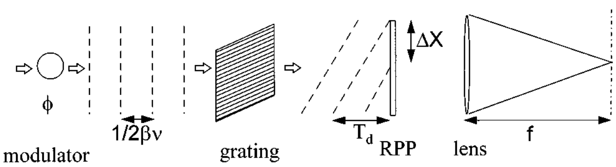

Fig. 1. Standard implementation of 1D SSD.

B. Statistical Analysis

Our goal is to show that statistical theory may be used to perform an efficient study of the smoothing performances of the different methods introduced above. From a practical point of view, the fluence distribution over some surface Σ is examined: $(I(t, x))_{x\in\Sigma}$. We introduce the spatial measure, denoted by μ, that connects to any functional $f(I)$ the spatial average $\int_\Sigma f(I)(x)\mathrm{d}x/|\Sigma|$. So we are looking for data on the measure μ, which depends on the realization of the pattern that is observed. From a theoretical point of view, we are going to carry out statistical averages with respect to the possible realizations of the patterns, which correspond to the possible realizations of the experimental devices. The randomness holds in the fluctuations of the radius or the index of refraction of the fiber core in the SOF case and in the random phases imposed by the elements of the RPP in the SSD case. This average is denoted by $\langle\cdot\rangle$ and carried out in some fixed point x in Σ. If the field is spatially ergodic, then the spatial measure μ and the statistical measure $\langle\cdot\rangle$ coincide for a well-chosen surface Σ, where the field is macroscopically similar but microscopically moving. It is equivalent to compute a statistical average over all possible realizations at some fixed point x and to compute a spatial average over $x \in \Sigma$ for some given realization. That will actually be the case in the configurations that will be examined throughout the paper.

C. Generation of Long Broadband Pulses

Ideally, the spectral broadening is obtained by imposing a phase modulation on the monochromatic incident beam. Such a method is of great interest for the technique of SSD. Indeed, in (and near) the relay image planes of the gratings, the pure phase modulation does not induce any amplitude modulation. As a consequence, if the amplifiers lie in these planes, the amplification performance is equivalent to that of a smooth, clean beam. On the other hand, in the SOF configuration, because of unavoidable large spatial fluctuations in intensity, nonlinear effects such as self-phase modulation and filamentation may develop with induced reduction of amplification.[9] In this paper, to make the comparison meaningful, we compare the smoothing performances of the SSD and SOF techniques with the same spectral broadenings. So we shall assume in the following that similar phase modulators are used in the SSD and SOF configurations. We shall consider in this paper two phase modulation methods. We shall use, on the one hand, the pure sinusoidal phase modulator

$$\phi_{\mathrm{spm}}(t) = \beta \sin(2\pi\nu t), \tag{1}$$

with depth β and frequency ν, and, on the other hand, the random phase modulator ϕ_{rpm}, which is assumed to obey stationary Gaussian statistics, with mean 0 and Gaussian correlation function, i.e.,

$$\mathbb{E}[\phi_{\mathrm{rpm}}(t)] = 0,$$

$$\mathbb{E}[\phi_{\mathrm{rpm}}(t)\phi_{\mathrm{rpm}}(t')] = \sigma^2 \exp[-\omega_c{}^2(t-t')^2], \tag{2}$$

where $\mathbb{E}$ stands for statistical averaging with respect to the distribution of the process f. Such a process is time ergodic, so that the time average $\langle \cdot \rangle_t$ coincides with $\mathbb{E}$. The production of modulations with random properties will be discussed in Subsection 4.C. In what follows we shall compare the performances of sinusoidal and random modulators. So it is convenient to establish the relations between the scalars that characterize them. An efficient way consists of analyzing the autocorrelation functions:

$$\begin{aligned}\langle \phi_{\text{spm}}(t)\phi_{\text{spm}}(t+\Delta t)\rangle_t &= (\beta^2/2)\cos(2\pi\nu\Delta t)\\ &\simeq (\beta^2/2)(1-2\pi^2\nu^2\Delta t^2)\\ &\qquad \text{if } \nu\Delta t \ll 1,\\ \mathbb{E}[\phi_{\text{rpm}}(t)\phi_{\text{rpm}}(t+\Delta t)] &= \sigma^2 \exp(-\omega_c{}^2\Delta t^2)\\ &\simeq \sigma^2(1-\omega_c{}^2\Delta t^2)\\ &\qquad \text{if } \omega_c\Delta t \ll 1. \end{aligned} \tag{3}$$

Therefore in the comparisons it will be consistent to identify $\beta = \sqrt{2}\sigma$ and $\sqrt{2}\pi\nu = \omega_c$. If these relations are taken into account, a sinusoidal modulator and a random modulator involve spectral broadenings whose full-bandwidth extents are similar. However, it should be emphasized that a sinusoidal phase modulator with frequency ν and depth β produces a discrete spectrum consisting of approximately 2β lines separated by $2\pi\nu$, whereas a random phase modulator produces a continuous spectrum of full-bandwidth extent (FWHM) $\sim 2\sqrt{\ln 2}\sigma\omega_c$.

The spectral filling uniformity will appear essential for the smoothing efficiency. Regardless of the method, the coherence time of a beam with full bandwidth $\Delta\nu$ is equal to $1/\Delta\nu$. Thus the maximal reduction of the contrast for time integration T is $\sqrt{\Delta\nu T}$. It appears that the larger the bandwidth, the more rapid the reduction of the contrast.[8] However, the full-bandwidth extent is not the single determinant parameter. Another important parameter is the number $N_{\max}$ of uncorrelated speckle patterns that can be generated by a beam with bandwidth $\Delta\nu$. If the spectrum is continuous, then $N_{\max}$ is given by the ratio $\Delta\nu/\delta\nu_{\text{ind}}$, where $\delta\nu_{\text{ind}}$ is the minimum frequency shift required to decorrelate the speckle patterns generated by two monochromatic beams of different frequencies. $\delta\nu_{\text{ind}}$ depends only on the dispersive device of the selected smoothing method and is inversely proportional to the induced time delay. If the spectrum is discrete, $N_{\max}$ may be inferior to the ratio $\Delta\nu/\delta\nu_{\text{ind}}$ because the holes in the spectrum obviously cannot generate any speckle pattern. So a more adequate and general definition of $N_{\max}$ is the number of spectral bands of bandwidth $\delta\nu_{\text{ind}}$ that can be inserted in the effective spectrum.

As an example, we can consider the spectral broadening generated by a sinusoidal phase modulator. We deal with approximately 2β monochromatic lines whose frequencies are separated by ν. If $\nu > \delta\nu_{\text{ind}}$, then the speckle patterns generated by the lines of the spectrum are uncorrelated. We can set one band with bandwidth $\delta\nu_{\text{ind}}$ on every line, so $N_{\max}$ is equal to 2β and the asymptotic contrast reduction will be equal to approximately $\sqrt{2\beta}$. If $\nu < \delta\nu_{\text{ind}}$, then the speckle patterns generated by the lines of the spectrum are correlated. The discrete spectrum is actually equivalent to a continuous spectrum because the dispersive device does not resolve the lines. Then $N_{\max}$ is given by the ratio $2\beta\nu/\delta\nu_{\text{ind}}$, which is inferior to 2β.

D. Asymptotic Framework

The results presented in what follows are valid in the asymptotic framework of a large number of elements of the RPP in the case of SSD or of excited optical modes of the fiber in the case of SOF. Within this framework some limit theorems can be applied, namely, the strong law of large numbers and the central limit theorem,[10] which simplify the expressions of the contrasts and the correlation functions of the smoothed patterns.

Throughout the paper we shall give general expressions and not discuss the actual constraint of the angular spread of the pulse imposed by the laser divergence. It is relevant for applications to check *a posteriori* that the parameters that are used as entries in these formulas can meet the constraint imposed by the laser divergence. On the other hand, the meaning of this constraint depends on the selected method. In the SSD configuration the number of speckle spots is imposed by the number of elements of the RPP and is independent of the time delay, which depends on the gratings and is proportional to the angular spread of the beam. In the SOF configuration the number of speckle spots is given by the number of modes of the fiber and is limited by the acceptable angular spread of the beam, while the time delay is proportional to the length of the fiber. As a consequence, whatever the laser divergence is, the time delay for SOF can be made as long as desired, in fact of the same order as that of the pulse duration.

We shall say just a few words about the nonlinear frequency conversion, which is expected to be associated with smoothed beams.[2] On the one hand, this implies convolution distortion to the far-field spot,[11] which affects both the statistics and the envelope of the focal spot in a way that can be easily computed. On the other hand, the efficiency of the frequency tripling is related mainly to the full-bandwidth extent of the pulse. As pointed out in Subsection 2.C, to make the comparison meaningful, we compare the smoothing performances of the SSD and SOF techniques with the same spectral broadenings. As a consequence, the frequency conversion efficiencies are not expected to be very different for the SOF and SSD techniques with equivalent divergences and bandwidths.

3. SMOOTHING BY SPECTRAL DISPERSION

A. Implementation

It appears that smoothing by 1D SSD is insufficient to reach the required level of uniformity for direct-drive inertial confinement fusion. On the one hand, we cannot expect to obtain the required contrast reduction of 1%,[1] even if we take into account the overlap of approximately 200 beams on the target in the NIF (Ref. 8) and LMJ (Ref. 3) configurations. On the other hand, only the spatial frequencies in the dispersion direction are smoothed. The performance of SSD can be greatly improved if the beam is dispersed in both orthogonal directions. A straightforward implementation of 2D SSD is shown in Fig. 2.[8] The spectral dispersion is obtained by applying a phase modulator and then a grating in each orthogonal direction. An auxiliary grating is imposed before each modulator to compensate for the temporal skew of the global shape E_0 of the field. We assume that the input beam is a monochromatic pulse with pulsation ω_0 and duration T_{pulse} (longer than all the characteristic time scales involved in the problem), and we consider pure sinusoidal phase modulators. After modulation and dispersion the field is

$$E_1(t, x, y) = E_0(t)\exp\{i[\phi_1(t + s_1 x) + \phi_2(t + s_2 y)]\}, \tag{4}$$

where ϕ_j is the phase modulation and s_j is the temporal skew per unit length generated by the gratings in the x direction for $j = 1$ and in the y direction for $j = 2$. In the focal plane of the lens, the fields of the beamlets overlap:

$$\begin{aligned} E(t, x, y) = {} & \frac{1}{2\pi}\int_{-\infty}^{+\infty} \mathrm{d}\omega \sum_{j,l} E_{1,j,l}(\omega) \\ & \times \exp\left(-ijx\,\frac{2\pi h}{\lambda_0 f}\right)\exp\left(-ily\,\frac{2\pi h}{\lambda_0 f}\right) \\ & \times \exp(i\phi_{j,l})\exp(i\omega t), \end{aligned} \tag{5}$$

where λ_0 is the carrier wavelength of the incident wave, D is the near-field square beam aperture, f is the lens focal length, and h is the length of the side of a square element of the RPP. We denote by N^2 the number of elements of the square RPP, i.e., $N = D/h$. $\phi_{j,l}$ is the random phase imposed by the (j, l)th element. We assume that the $\phi_{j,l}$ are independent random processes that may take the value 0 or π with probability 1/2. The field that illuminates the (j, l)th element is $E_{1,j,l}(t) = E_1(t, s_1 jh, s_2 lh)$. We consider points in the focal plane such that $x,y < \lambda_0 f/h$, so that the smooth sinc envelope of the diffraction function of a square aperture can be considered as quasi-uniform. If N^2 is large, the field E is a stationary, centered, Gaussian process. Throughout the paper we normalize the mean intensity, so that we assume that it is equal to 1. The correlation function of intensities is defined by

$$\Gamma(t, x, y; t', x', y') = \langle I(t, x, y)I(t', x', y')\rangle. \tag{6}$$

In the 2D SSD case and in the limit $N \to \infty$, it is shown in Appendix A that the correlation function of intensities is separable in the two orthogonal dispersion directions:

$$\begin{aligned} & \Gamma(t, x, y; t', x', y') \\ & \quad = 1 + \Gamma_1(t, x; t', x')\Gamma_2(t, y; t', y'), \end{aligned} \tag{7}$$

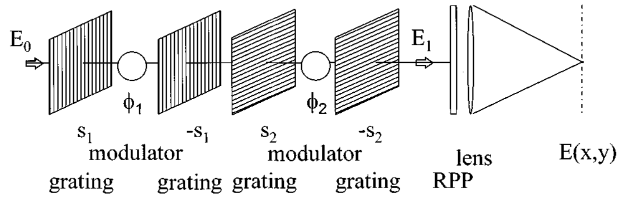

Fig. 2. Standard implementation of 2D SSD.

with

$$\begin{aligned} \Gamma_j(t, z; t', z') = \int_{-1/2}^{1/2} & \mathrm{d}s\ \exp\{i[\phi_j(t + T_{dj}s) \\ & - \phi_j(t' + T_{dj}s) - 2\pi s(z - z')/r_c]\}, \end{aligned}$$

where the T_{dj} are the time delays induced by the gratings and r_c is the correlation radius of the speckle pattern, i.e.,

$$T_{dj} = s_j D, \qquad r_c = \lambda_0 f/D. \tag{8}$$

As a numerical example, we can consider the NIF geometry[2]: $D = 0.35$ m, $F = 7$ m, and $\lambda_0/D = 1\ \mu$rad (at 351 nm). The characteristic radius of the speckle spots, r_c, is then approximately 7 μm, while the size of the focal spot is of the order of 500 μm. Moreover, the typical values for the lateral time delays imposed by the gratings are of the order of 200 ps.

B. Sinusoidal Modulations

We consider in this subsection pure sinusoidal phase modulators $\phi_j(t) = \beta_j \sin(2\pi\nu_j t)$, where β_j and ν_j are, respectively, the modulation depth and frequency of the jth modulator. We aim at studying the properties of the smoothed pattern obtained by integrating the intensity over rather long times. Long times means longer than the modulation periods. The correlation function of intensities of the smoothed speckle pattern is computed by averaging the correlation function Γ of the instantaneous speckle pattern defined by Eq. (6) with respect to both t and t'. It admits a simple and separable expression when ν_1 and ν_2 are incommensurate:

$$\Gamma_s(x, y; x', y') = 1 + \Gamma_{s1}(x' - x)\Gamma_{s2}(y' - y), \tag{9}$$

with

$$\Gamma_{sj}(\Delta z) = \sum_{n=-\infty}^{+\infty} a_n(\beta_j)\mathrm{sinc}^2(\nu_j T_{dj} n - \Delta z/r_c),$$

where the positive coefficients $a_n(\beta)$ depend only on the modulation depth β and can be expressed by means of the Bessel functions as

$$a_n(\beta) = \sum_{m=-\infty}^{+\infty} J_{m+n}{}^2(\beta) J_m{}^2(\beta). \tag{10}$$

The smoothed contrast is given by $[\Gamma_s(x, y; x, y) - 1]^{1/2}$ and is plotted in Fig. 3. When $\nu_j T_{dj} \geqslant 1$, $j = 1, 2$, the contrast reduction is optimal:

$$c^2(\beta_1, \beta_2) = a_0(\beta_1)a_0(\beta_2). \tag{11}$$

The condition $\nu T_d \geqslant 1$ means that the modulator effectively modulates over the time delay induced by the gratings. As a consequence, the dispersive device (constituted by the gratings) resolves the lines of the spectrum of the modulated beam. The speckle patterns generated by the lines of the spectrum are uncorrelated, which produces an optimal contrast reduction.

On the contrary, if $\nu T_d < 1$, then the modulation period is longer than the time delay of the gratings. The shift frequency required to decorrelate the speckle patterns in the target plane is larger than the interval between successive lines of the spectrum. Thus the speckle

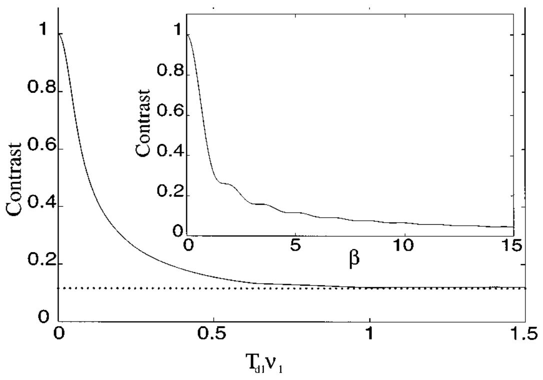

Fig. 3. Asymptotic contrast: 2D SSD with sinusoidal modulations. The optimal contrast (11) is plotted in the inset as a function of β (when $\beta_1 = \beta_2 = \beta$). The asymptotic contrast $[\Gamma_s(x, y; x, y) - 1]^{1/2}$ is plotted as a function of $\nu_1 T_{d1}$ when $\beta_1 = \beta_2 = 5$. The dotted line represents the optimal contrast (11) corresponding to $\nu_j T_{dj} \geqslant 1$.

patterns generated by the lines are slightly correlated, which affects the smoothing efficiency and increases the contrast.

Let us quantify the smoothed fluence distribution. Correlation peaks regularly spaced in both orthogonal dispersion directions can be seen in the correlation function. This structure is made evident by examining the smoothed power spectral density (PSD) $\mathscr{G}_s(\nu_x, \nu_y)$. As implied by the Wiener–Khintchine theorem,[10] the PSD is given by the 2D Fourier transform of the correlation function Γ_s. We obtain

$$\mathscr{G}_s(\nu_x, \nu_y) = \delta(\nu_x, \nu_y) + {r_c}^2 G_{s1}(r_c \nu_x) G_{s2}(r_c \nu_y), \tag{12}$$

with

$$G_{sj}(\alpha) = \Lambda(\alpha) {J_0}^2(\sqrt{2}\beta_j[1 - \cos(2\pi\nu_j T_{dj}\alpha)]^{1/2}),$$

where $\Lambda(\alpha) = 1 - |\alpha|$ if $|\alpha| \leqslant 1$ and $\Lambda(\alpha) = 0$ if $|\alpha| > 1$. The PSD's are plotted in Fig. 4. We can distinguish two regimes. First, if $\nu_j T_{dj} \leqslant 1$, then the spatial spectrum presents a unique central peak, which shows that only the spatial frequencies above $h_0/(2\pi\beta\nu_j T_{dj} r_c)$ ($j = 1$ in the x direction and $j = 2$ in the y direction) are smoothed [$h_0 \simeq 1.1$ is such that $J_0(h_0) = 1/\sqrt{2}$]. Second, if $\nu_j T_{dj} > 1$, the spatial frequencies below $h_0/(2\pi\beta\nu_j T_{dj} r_c)$ ($j = 1$ in the x direction and $j = 2$ in the y direction) are not smoothed. Moreover, the spectrum appears concentrated near some particular spatial frequencies, which are multiples of $\Delta\nu_x = 1/(\nu_1 T_{d1} r_c)$ in the x direction and of $\Delta\nu_y = 1/(\nu_2 T_{d2} r_c)$ in the y direction. This is due to the use of pure sinusoidal modulation; a more advanced phase modulation will break this resonant structure. As a consequence, a smoothed pattern looks like a rectangular array of regularly spaced spots of size r_c, separated in the x direction by $\Delta x = \nu_1 T_{d1} r_c$ and in the y direction by $\Delta y = \nu_2 T_{d2} r_c$. We can easily check that these results are consistent with the heuristical arguments of Subsection 2.A.

It is convenient to study the properties of the smoothed speckle pattern for integration times shorter than the modulation periods, with arbitrary modulation frequencies. The smoothed contrast $c(T)$ is given by $[\Gamma_T(x, y; x, y) - 1]^{1/2}$, where $\Gamma_T = \int_0^T \int_0^T \Gamma \, \mathrm{d}t \mathrm{d}t'/T^2$. Its exact expression is the following:

$$c^2(T) = \sum_{m,n=-\infty}^{+\infty} \mathrm{sinc}^2[(m\nu_1 + n\nu_2)T] a_m(\beta_1) a_n(\beta_2), \tag{13}$$

where $a_n(\beta)$ has been defined by Eq. (10). When the frequency modulations are incommensurate, the contrast (13) decreases as $\sqrt{T}$ for small integration times T. More exactly, if ν_1 and ν_2 are close to the same value ν and incommensurate, then the contrast decreases roughly as $\sqrt{4\beta\nu T}$ for small integration times T until it reaches the asymptotic value (11) for integration times of the order of β/ν. Figure 5 represents the evolution of the smoothed contrast as a function of the integration time T for different modulation frequencies. When the frequencies are commensurate [the case ($\nu_1 = 1$ GHz, $\nu_2 = 1$ GHz) or the case ($\nu_1 = 1$ GHz, $\nu_2 = 2$ GHz) in Fig. 5], then the inte-

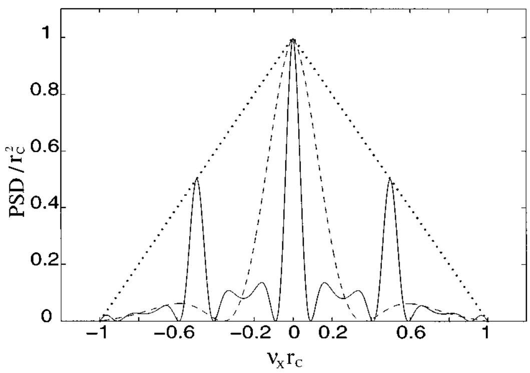

Fig. 4. Normalized power spectral densities (PSD's) in the x direction: 2D SSD for different sinusoidal modulations. The dotted curve represents the density of the instantaneous speckle pattern. The densities of the smoothed patterns are plotted as a dashed curve in the case $T_{d1}\nu_1 = 0.5$ and as a solid curve in the case $T_{d1}\nu_1 = 2$. The modulation depth is taken to be equal to 5. The Dirac function, which is due to the nonzero mean intensity of the speckle pattern, is not plotted.

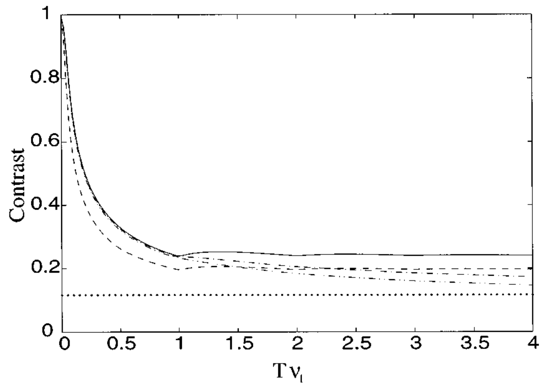

Fig. 5. Variation of the contrast with integration time: 2D SSD with different sinusoidal modulations, with $\beta_j = 5$ and $\nu_j T_{dj} = 1$ for $j = 1, 2$. The dotted line represents the asymptotic optimal contrast (11). The solid, dashed, dotted–dashed, and dotted–dotted–dashed curves plot the cases ($\nu_1 = 1$ GHz, $\nu_2 = 1$ GHz), ($\nu_1 = 1$ GHz, $\nu_2 = 2$ GHz), ($\nu_1 = 1$ GHz, $\nu_2 = 1.05$ GHz), and ($\nu_1 = 1$ GHz, $\nu_2 = 1.1$ GHz), respectively.

grated contrast never reaches the optimal value Eq. [(11)] but stops at some higher value. Moreover, if we compare the case ($\nu_1 = 1$ GHz, $\nu_2 = 1.05$ GHz) with the case ($\nu_1 = 1$ GHz, $\nu_2 = 1.1$ GHz), it appears that the contrast reduction in the second one is more rapid, because the modulation frequencies in the first configuration are too close to each other.

C. Random Modulations

We aim now at studying the 2D SSD implementation of Fig. 2 when using statistically independent random phase modulators with equal parameters σ and ω_c. To simplify the notation, we shall assume, moreover, that the time skews per unit length generated by the gratings are both equal to s, so that each grating introduces the same time delay $T_d = sD$. We also assume that $\sigma\omega_c T_d > 1$, which means that the full-bandwidth extent $\sim 2\sqrt{\ln 2}\sigma\omega_c$ is larger than the frequency shift necessary to decorrelate the speckle pattern. The PSD of the smoothed speckle pattern for integration time T such that $\sigma\omega_c T > 1$ can then be expressed in a closed-form expression:

$$\mathscr{G}_T(\nu_x, \nu_y) = \delta(\nu_x, \nu_y) + r_c{}^2\Lambda(r_c\nu_x)\Lambda(r_c\nu_y) \times \Psi_T(r_c\nu_x, r_c\nu_y), \tag{14}$$

with

$$\Psi_T(\alpha_x, \alpha_y) = 2\int_0^1 \mathrm{d}s(1 - s)\psi(\omega_c T_d\alpha_x, \omega_c Ts) \times \psi(\omega_c T_d\alpha_y, \omega_c Ts),$$

where

$$\psi(u,v) = \exp(-\sigma^2\{2 - 2\exp(-u^2) - 2\exp(-v^2) + \exp[-(u - v)^2] + \exp[-(u + v)^2]\}),$$

and $\Lambda(\alpha) = 1 - |\alpha|$ if $|\alpha| < 1$ and $\Lambda(\alpha) = 0$ otherwise. This complicated formula is plotted in Fig. 6. When the integration time belongs to the interval $[1/(\sigma\omega_c), 1/\omega_c]$, it appears that the frequencies below $\sqrt{\ln 2}/(\sqrt{2}\sigma\omega_c{}^2T_dTr_c)$ are not yet smoothed. After this transition regime, i.e., for integration times T such that $\omega_c T > 1$, the spatial frequencies above $\sqrt{\ln 2}/(\sqrt{2}\sigma\omega_c T_d r_c)$ are smoothed according to the expected rate $\sqrt{T}$. In particular, the coherent resonance in the spatial spectrum exhibited by formula (12) in the case of sinusoidal modulations is smoothed. However, the frequencies below $\sqrt{\ln 2}/(\sqrt{2}\sigma\omega_c T_d r_c)$ are very poorly smoothed. Formula (14) can be somewhat simplified if $\omega_c T > 1$ and if $\sigma > 2$ [so that $\psi(u, v) \simeq 0$ when $u, v > 1$]:

$$\mathscr{G}_T(\nu_x, \nu_y) = \delta(\nu_x, \nu_y) + r_c{}^2\Lambda(r_c\nu_x)\Lambda(r_c\nu_y) \times \sup\left[\frac{\sqrt{\pi}\gamma_1}{\sigma\omega_c T}, \chi(\omega_c T_d r_c\nu_x)\chi(\omega_c T_d r_c\nu_y)\right], \tag{15}$$

where $\gamma_1 \simeq 1.25$ and $\chi(\alpha) = \exp\{-2\sigma^2[1 - \exp(-\alpha^2)]\}$. It should be emphasized that Eq. (15) is a simplified version of the exact expression (14). It holds true when $\omega_c T > 1$ and when one of the terms in the supremum argument is clearly larger than the other. Integrating the PSD over the spatial frequencies, we can deduce the contrast:

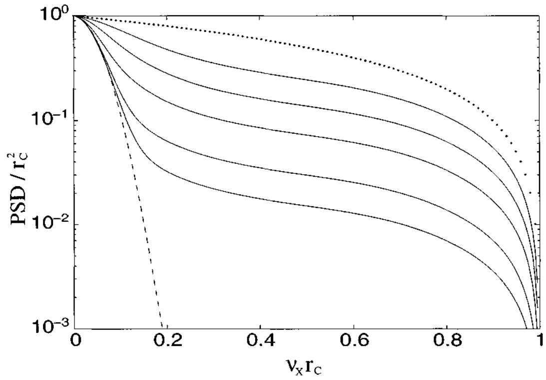

Fig. 6. Normalized PSD's: 2D SSD with random modulations. The dotted curve represents the density of the unsmoothed pattern. The densities of the smoothed patterns integrated over $T = 0.5/\omega_c$, $T = 1/\omega_c$, $T = 2/\omega_c$, $T = 5/\omega_c$, and $T = 10/\omega_c$ are successively plotted (from top to bottom) as solid curves. The dashed curve represents the asymptotic PSD, which corresponds to an infinite pulse duration and an infinite integration time. The modulation amplitude is taken to be equal to $\sigma = 5/\sqrt{2}$, and the time delay $T_d = 3/\omega_c$.

$$c^2(T) = \frac{\pi\gamma_1{}^2}{2\sigma^2\omega_c{}^2T_d{}^2} + \frac{\sqrt{\pi}\gamma_1}{\sigma\omega_c T}. \tag{16}$$

4. SMOOTHING BY OPTICAL FIBER

A. Implementation

A broadband source illuminates a long multimode fiber. Although a natural broadband source is generally used in this configuration, for better comparison we consider a monochromatic source spectrally broadened by a phase modulator. The implementation is represented in Fig. 7. The incident beam excites many optical modes, which propagate according to different velocities. Moreover, small random fluctuations of the core radius or of the index of refraction affect the propagation by introducing random phases into the modes. If the fiber is long enough, these phases can be considered as independent processes that obey uniform distributions over $[0, 2\pi]$.[12] As a consequence, the optical modes interfere at the output of the fiber, and their overlap produces a speckle pattern. If the propagation in the amplifier chain is linear, then the properties of the speckle pattern on the target are the same as those at the output of the fiber. We shall give the results in the case of a square fiber, owing to the simplicity of the expressions of their modes. The field at the output of the fiber is then given by

$$E(t, x, y) = \frac{1}{2\pi}\int_{-\infty}^{+\infty} \mathrm{d}\omega \sum_{j,l} a_{j,l}(\omega)E_1(\omega)R_j(x)R_l(y) \times \exp[-i\beta_{j,l}(\omega)L + i\phi_{j,l} + i\omega t], \tag{17}$$

where ω_0 is the carrier pulsation of the incident wave, L is the length of the fiber, and a is its radius. R_j is the jth optical mode of the fiber in the x or y direction. $\phi_{j,l}$ is the random phase of the (j, l)th mode. We assume that the $\phi_{j,l}$ are independent random processes that obey uni-

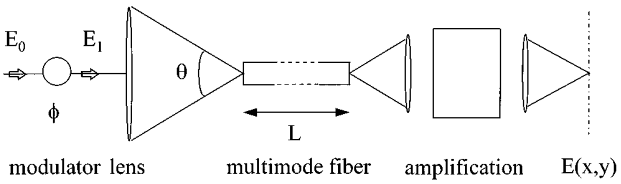

Fig. 7. Standard implementation of SOF.

form distributions over $[0, 2\pi]$.[12] $a_{j,l}$ is the decomposition of the input beam onto the (j, l)th mode. $E_1(\omega)$ is the Fourier transform of the phase-modulated field $E_0(t)\exp[i\phi(t)]$. The modes are[13]

$$R_j(x) = \begin{cases} \cos[j\pi x/(2a)] & \text{if } j \text{ is odd} \\ \sin[j\pi x/(2a)] & \text{if } j \text{ is even} \end{cases}. \tag{18}$$

$\beta_{j,l}$ is the positive solution of the dispersion equation

$$\beta_{j,l}{}^2(\omega) + (j^2 + l^2)\pi^2/(4a^2) = (n\omega/c)^2, \tag{19}$$

where n is the index of the core. The fiber is illuminated through the incidence angle θ, so that we assume that (j, l) modes satisfying $j^2 + l^2 \leqslant N^2$, with $N = na\omega_0\theta/(\pi c)$, are equally excited. If the number of excited modes, N^2, is large, then the field E obeys centered, stationary, and Gaussian statistics. Assuming that the direct mode emerges from the fiber from time 0 to time T_{pulse} and that the time delay is smaller than the pulse duration, the mean intensity is constant over $[T_d, T_{\text{pulse}}]$. Over this time interval the correlation function of intensities is

$$\Gamma(t, x, y; t', x', y') = 1 + \left| \int_{s=0}^{1} \mathrm{d}\alpha\, J_0(\pi\sqrt{s}r/r_c) \times E_1(t - sT_d)E_1^*(t' - sT_d) \right|^2, \tag{20}$$

where $r^2 = (x - x')^2 + (y - y')^2$. T_d and r_c are, respectively, the time delay induced by the fiber and the correlation radius of the pattern at the end of the fiber:

$$T_d = L\theta^2/(8nc), \qquad r_c = \lambda_0/\theta. \tag{21}$$

Such an approach has been experimented on the Phebus laser.[6] In the implemented geometry, $\theta \simeq 20$ deg, $a = 100\ \mu$m, and $L = 100$ m. As a consequence, the radius of the speckle spots in the fiber output pattern is approximately 3 μm (at 1053 nm). However, this plane is imaged on target with a factor-of-5 magnification, so that the radius of the speckle spots in the target plane is approximately 5 μm (at 351 nm). Finally, the time delay generated by the fiber is of the order of 5 ns.

B. Sinusoidal Modulations

To compare the respective smoothing performances of 2D SSD and of SOF, we shall assume that the phase modulator ϕ consists of the same modulators as those considered for 2D SSD. So we first assume in this subsection that $\phi(t) = \beta_1 \sin(2\pi\nu_1 t) + \beta_2 \sin(2\pi\nu_2 t)$, where β_j is the depth and ν_j is the frequency of the jth modulator. Assuming that $T_{\text{pulse}} > T_d$, the intensity distribution is temporally stationary over the time interval $[T_d, T_{\text{pulse}}]$. That will be our framework. The correlation function is equal to

$$\Gamma(t, x, y; t', x', y') = 1 + \gamma(t - t')\left[2\frac{J_1(\pi r/r_c)}{\pi r/r_c}\right]^2, \tag{22}$$

with

$$\gamma(\Delta t) = J_0{}^2(\sqrt{2}\beta_1[1 - \cos(2\pi\nu_1\Delta t)]^{1/2}) \times J_0{}^2(\sqrt{2}\beta_2[1 - \cos(2\pi\nu_2\Delta t)]^{1/2}),$$

where $r^2 = (x - x')^2 + (y - y')^2$. This result holds true when the frequencies ν_1 and ν_2 are incommensurate and when $T_d\nu_j \gg 1$. The last condition is obviously fulfilled with standard integrated optic phase modulators because of the long time delay induced by the fiber. The SOF method always takes place in the optimal situation, in which the phase modulators effectively modulate over the time delay of the dispersive device, so that it resolves the lines of the discrete spectrum. The interval between successive lines is much longer than the frequency shift required to decorrelate the speckle pattern; thus each line can generate an uncorrelated speckle pattern. The striking point is that the spatial and temporal variables are separable in the expression of the correlation function [Eq. (22)]. That means that this method generates completely uncorrelated speckle patterns instead of a speckle pattern that shifts as in the SSD implementation.

Let us study the properties of the smoothed pattern over integration time T. The correlation function of intensities is equal to

$$\Gamma_T(x, y; x', y') = 1 + c^2(T)\left[2\frac{J_1(\pi r/r_c)}{\pi r/r_c}\right]^2, \tag{23}$$

where the contrast $c(T)$ is given by Eq. (13). If the integration time is longer than the modulation frequencies, then we get the asymptotic contrast (11). So it appears that the contrasts of the patterns smoothed by 2D SSD and by SOF are similar. However, the spatial spectra are very different. While the smoothing rate depends strongly on the spatial frequency for SSD, the striking point is that SOF smoothes all spatial frequencies equally. Indeed, the PSD is given by

$$\mathscr{G}_T(\nu_x, \nu_y) = \delta(\nu_x, \nu_y) + c^2(T)r_c{}^2G(r_c\sqrt{\nu_x{}^2 + \nu_y{}^2}), \tag{24}$$

where $G(x) = (8/\pi^2) \times (\arccos x - x\sqrt{1 - x^2})$ if $x \in [0, 1]$ and $G(x) = 0$ otherwise and is plotted in Fig. 8. The results that have been presented above hold true in the approximation $\nu T_d \gg 1$. If we take into account the finite parameter νT_d, then the results are modified in the following way. The correlation function and the contrast are given by Eq. (23) up to a term of the order of $1/(2\beta\nu T_d)$. The PSD is given by Eq. (24) for spatial frequencies above $1/(2\beta\nu T_d r_c)$. Spatial frequencies below this are not actually smoothed. However, if we adopt phase modulators with frequencies 10 GHz and depth 5 combined with a 100-m-long fiber, which generates a 5-ns time delay, then only the spatial frequencies below $1/(500 r_c)$ would not be smoothed. This frequency band is far from the frequencies that can be resolved, since they

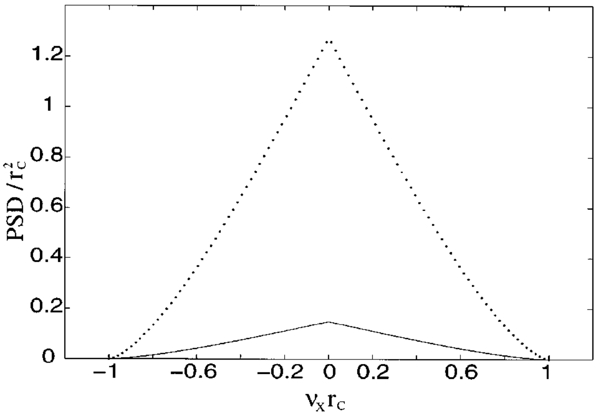

Fig. 8. Normalized PSD's: SOF with two sinusoidal modulators with depth 5 and incommensurate frequencies. The dotted (solid) curve represents the density of the unsmoothed (smoothed) pattern.

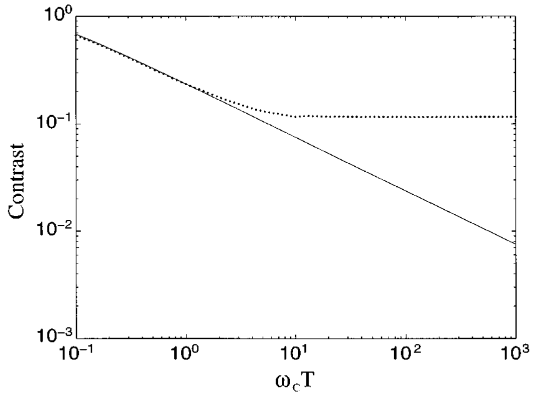

Fig. 9. Variation of the contrast with time integration: SOF. The solid line corresponds to a phase modulation generated by two independent random modulators with equal parameters $\sigma = 5/\sqrt{2}$ and ω_c. The dotted curve plots the contrast reduction when using two sinusoidal phase modulators with depth $\beta = 5$ and frequencies $\nu_1 = 0.9\omega_c/(\sqrt{2}\pi)$ and $\nu_2 = 1.1\omega_c/(\sqrt{2}\pi)$, respectively.

correspond to spatial sizes of several millimeters, which are larger than the fiber output or the focal spot. So we can consider that the above results hold true for the relevant frequencies.

C. Random Modulations

We now assume that the phase modulator ϕ consists of two statistically independent random phase modulators ϕ_{rpm1} and ϕ_{rpm2} with equal parameters σ and ω_c. The correlation function of the instantaneous intensity is given by Eq. (20), with

$$E_1(t) = E_0(t)\exp\{i[\phi_{\mathrm{rpm1}}(t) + \phi_{\mathrm{rpm2}}(t)]\}.$$

Integrating with respect to both t and t', we find that the correlation function of the integrated intensity for an integration time T is equal to Eq. (23), where the contrast admits the following expression when $\sigma\omega_c T > 1$:

$$c^2(T) = \exp(-4\sigma^2) + \frac{\sqrt{\pi}}{\omega_c T} f_1(\sigma) - \frac{1}{{\omega_c}^2 T^2} f_2(\sigma). \tag{25}$$

The functions

$$f_j(\sigma) = \exp(-4\sigma^2) \sum_{n=1}^{\infty} (4\sigma^2)^n/(n!n^{j/2})$$

can be simplified when $\sigma > 2$, so that we get

$$c^2(T) = \frac{\sqrt{\pi}\gamma_1}{\sigma\omega_c T}, \tag{26}$$

where $\gamma_1 \simeq 1.25$. So the contrast decreases according to the expected $\sqrt{T}$ rate. Indeed, N uncorrelated speckle patterns are generated during a time interval of duration T, where N is proportional to $\sigma\omega_c T$, and the contrast decreases as $\sqrt{N}$. If the integration time is as long as the time delay generated by the fiber, then the contrast reaches its minimal value. It is also interesting to remark that the contrast reductions obtained by either random or sinusoidal modulations are similar for small integration times, as shown by Fig. 9. But for integration times longer than β/ν, the contrast obtained with sinusoidal modulations reaches its asymptotic value (11), while the contrast obtained with random modulations goes on decreasing according to the rate $\sqrt{T}$. Finally, spatial frequencies are equally smoothed, since this feature does not depend on the nature of the modulation. The PSD of the time-integrated intensity is given by Eq. (24) combined with the expression of contrast [Eq. (26)].

5. DISCUSSION

A. Best Choice among Sinusoidal Modulators

As an application of the above results, we study the respective contributions of the frequencies and the depths of the modulators in order to reduce the contrast. We consider the SOF configuration with one sinusoidal modulator with depth β and frequency ν, which is equivalent from a contrast point of view to the 1D SSD configuration satisfying the condition $T_d\nu \geqslant 1$. The contrast of the integrated pattern is then given by

$$c^2(T) = \sum_{n=-\infty}^{\infty} \mathrm{sinc}^2(n\nu T)a_n(\beta).$$

In particular, the asymptotic contrast $c^2 = a_0(\beta)$ depends only on the depth of the modulator. For the sake of convenience with respect to the smoothing performance, the phase modulator should have an amplitude as deep as possible, so as to get an important reduction of the asymptotic contrast, and a period as short as possible, so that the contrast can reach its asymptotic value quickly. Unfortunately, these constraints are difficult to meet simultaneously from an experimental point of view, because the electro-optic phase modulators are built so that when one increases their modulation depths, one also increases their periods. Figure 10 represents the variation of the contrast when using different sinusoidal modulators. The product $\beta\nu$ (proportional to the spectral broadening) of the modulator is set at some fixed value,

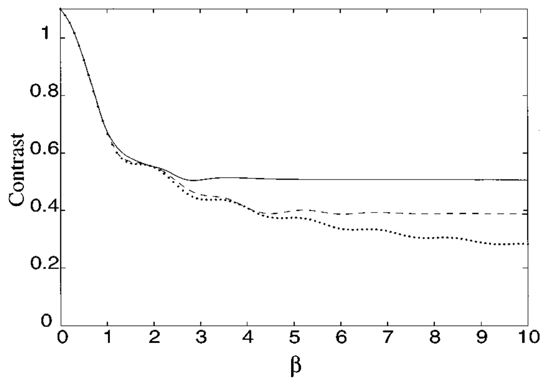

Fig. 10. Variation of the contrast with different sinusoidal modulators. The contrast is plotted as a solid curve for an integration time of 100 ps and a spectral broadening $2\beta\nu = 40$ GHz, and as a dashed curve for an integration time of 100 ps and a spectral broadening $2\beta\nu = 80$ GHz. The dotted curve corresponds to the asymptotic contrast.

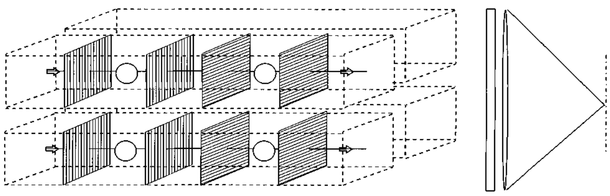

Fig. 11. Four-beam overlap configuration. Four broadband beams spectrally dispersed in both orthogonal directions illuminate a large RPP and focus on the target. Similar gratings are used for the dispersions of the beams. Only the phase modulations and/or the high carrier frequencies may differ. We assume also that the four beams have the same polarization.

but the depth β is varying and so is the period ν^{-1}. When the integration time is longer than the modulation period, the contrast is very close to the asymptotic value (zone $\beta < \beta\nu T$). On the other hand, when the integration time is shorter than the modulation period, the contrast becomes stable at some value (zone $\beta > \beta\nu T$). Indeed, two different effects are opposed to each other. First, the modulation period $1/\nu$ decreases, which induces a smoothing efficiency reduction, because the contrast has not enough time to reach its asymptotic value. Second, the modulation depth β increases, which implies a reduction of the value of the asymptotic contrast. When the product $\beta\nu$ is kept constant, these effects are exactly balanced. The global aspect of the curves of Fig. 10 is that the contrast decreases with β, which indicates that the modulation depth is the predominant parameter for smoothing performance. This conclusion is also supported by the arguments of Subsection 2.C, where we find that the filling uniformity of the bandwidth is favorable for smoothing.

B. Effects of Multiple-Beam Overlap

The results presented above hold for a single beam. In the NIF (Ref. 8) and LMJ (Ref. 3) direct-drive configurations, the whole target is illuminated by approximately 200 beams, and each point of the target by effectively approximately 50 beams. So it should be convenient to study the averaging effects of such an overlap. However, the overlapping fields may have different polarizations. This is consequently a delicate problem. In this paper we shall consider only the particular configuration described in Fig. 11. The overlap induces an increase of the final beam aperture, so that the correlation radius (i.e., the characteristic size of the speckle spots) of the instantaneous pattern is reduced by a factor of 2. If the high carrier frequencies are the same and similar modulators are applied on each beam, then the results of the above sections hold if we take care to replace r_c by $r_c/2$ and T_d by $2T_d$. As a consequence, the contrast reduction induced by the multiple-beam overlap is very poor. In particular, there is no further contrast reduction if sinusoidal modulators that fulfill the condition $\nu T_d \geqslant 1$ are used. If modulators are random, then the gain consists in a decrease by a factor of 2 of the limit spatial frequency below which there is no smoothing [see Eq. (14)], which implies a slight contrast reduction, since the first term in Eq. (16) is divided by 4. If different modulators are used and/or the high carrier frequencies of the beams are different, so that the corresponding spectra do not overlap, then the interference terms between the four beams average to 0, and the smoothed fluence is constituted by the sum of the four smoothed intensity distributions generated by the beams. As a result, the contrast of the smoothed pattern generated by the four beams is reduced by a factor of 2 with respect to that generated by a single beam, which corresponds to the smoothing of the highest spatial frequencies. So it appears in all cases that the spectra of the different beams need to be distinct to get a further contrast reduction. One can therefore take advantage of the beam multiplicity to broaden efficiently the total spectrum, while the spectral bandwidth extents of the individual beams are narrow enough to allow a good frequency conversion efficiency.

6. CONCLUSION

We have developed a statistical analysis for beam smoothing and have obtained closed-form expressions for the fluence distributions of the speckle patterns generated by different techniques. As an application, the comparison of the SOF and 2D SSD techniques produces evidence that each method has specific advantages and drawbacks. From the pure point of view of smoothing, SOF seems more efficient. Indeed, the cutoff frequency (below which the spatial frequencies are not smoothed) is inversely proportional to the time delay. Thus 2D SSD does not smooth a somewhat large band of low spatial frequencies, while SOF is able to smooth all relevant frequencies equally. However, the nonlinear propagation and the frequency conversion are expected to be drawbacks of SOF.

APPENDIX A

We aim to sketch the computation of the correlation functions of the instantaneous speckle patterns generated by 2D SSD and by SOF. The asymptotic results derived in this paper hold when the number of elementary fields that appear in the sums (5) and (17) is large. It follows from the central limit theorem[10] that as $N \to \infty$ the total field E obeys circular Gaussian statistics. We can then show that the correlation function of intensities defined by Eq. (6) can be easily deduced from the correlation function of fields. Indeed, for circular complex Gaussian fields, this relation is simply

$$\Gamma(t, x, y; t', x', y') = \langle |E(t, x, y)|^2 \rangle \langle |E(t', x', y')|^2 \rangle + |\langle E(t, x, y) E^*(t', x', y') \rangle|^2. \tag{A1}$$

So it remains to compute the correlation function of fields. The arguments are similar in the SSD and SOF cases, so we restrict our attention to SSD, where E is given by Eq. (5). We have

$$\langle E(t, x, y) E^*(t', x', y') \rangle = \frac{1}{4\pi^2} \sum_{j,l} \iint \mathrm{d}\omega \mathrm{d}\omega' \, E_{1,j,l}(\omega) E^*_{i,j,l}(\omega') \times \exp\left(i \left\{ \frac{2\pi h}{\lambda_0 f} [j(x - x') + l(y - y')] + \omega t - \omega' t' \right\} \right). \tag{A2}$$

In the asymptotic framework $N \to \infty$, we can replace the discrete sums by continuous integrals. If we first integrate with respect to ω and ω', then the Dirac functions $\delta(t - s)$ and $\delta(t' - s')$ appear, which yields Eq. (7). In the case of sinusoidal modulations, we can expand the exponential term $\exp(i\beta \sin\theta)$ in a Fourier series $\sum_{n=-\infty}^{\infty} J_n(\beta) \exp(in\theta)$, so that we get formulas (9) and (13) after time integration. In the case of random modulations, we use the strong law of large numbers to obtain Eq. (14).

ACKNOWLEDGMENTS

We thank J. Paye and C. Sauteret for useful and stimulating discussions and J. E. Rothenberg for making us preprints available. This work was performed under the auspices of the Laser MegaJoule Program of Commissariat à l'Energie Atomique/Direction des Applications Militaires (CEA/DAM) and the Groupement de Recherches "Propagation des Ondes en Milieux Aléatoires et/ou Non-linéaires" (GDR POAN) of Centre National de la Recherche Scientifique.

Address correspondence to J. Garnier at the address on the title page or tel: 33-1-6933-4630; fax: 33-1-6933-3011; e-mail: garnier@cmapx.polytechnique.fr.

REFERENCES

1. R. H. Lehmberg and S. P. Obenschain, "Use of induced spatial incoherency for uniform illumination," Opt. Commun. **46**, 27–31 (1983).
2. J. E. Rothenberg, "SSD with generalized phase modulation," Lawrence Livermore National Laboratory Rep. NIF-LLNL-96-02 (December 27, 1995), pp. 1–10.
3. M. André, "Megajoule solid state laser for ICF applications," in *Technical Committee Meeting on Drivers and Ignition Facilities for Inertial Fusion*, J. Coutant, ed., Proceedings of the International Atomic Energy Agency (CEA/DAM Publications, Limeil-Valenton, France, 1995), pp. 77–78.
4. R. H. Lehmberg, A. J. Schmitt, and S. E. Bodner, "Theory of induced spatial incoherence," J. Appl. Phys. **62**, 2680–2701 (1983).
5. S. Skupsky, R. W. Short, T. Kessler, R. S. Craxton, S. Letzring, and J. M. Soures, "Improved laser-beam uniformity using the angular dispersion of frequency-modulated light," J. Appl. Phys. **66**, 3456–3462 (1989).
6. D. Véron, H. Ayral, C. Gouédard, D. Husson, J. Lauriou, O. Martin, B. Meyer, M. Rostaing, and C. Sauteret, "Improved laser-beam uniformity using the angular dispersion of frequency-modulated light," Opt. Commun. **65**, 42–45 (1988).
7. J. W. Goodman, "Statistical properties of laser speckle patterns," in *Laser Speckle and Related Phenomena*, J. C. Dainty, ed., Vol. 9 of Topics in Applied Physics (Springer-Verlag, Berlin, 1984), pp. 9–75.
8. J. E. Rothenberg, "Two-dimensional smoothing by spectral dispersion for direct drive inertial confinement fusion," in *Solid State Lasers for Applications to ICF*, M. André and H. T. Powell, eds., Proc. SPIE **2633**, 634–644 (1995).
9. D. Véron, G. Thiell, and C. Gouédard, "Optical smoothing of the high power Phebus Nd-glass laser using the multimode optical fiber technique," Opt. Commun. **97**, 259–271 (1993).
10. D. Middleton, *Introduction to Statistical Communication Theory* (McGraw-Hill, New York, 1960).
11. R. H. Lehmberg, "Spatial profile distortion of harmonically-converted partially-coherent light," Opt. Commun. **130**, 51–56 (1996).
12. B. Moleshi, J. W. Goodman, and E. G. Rawson, "Bandwidth estimation for multimode optical fibers using the frequency correlation function of speckle patterns," Appl. Opt. **22**, 995–999 (1983).
13. A. Yariv, *Quantum Electronics* (Wiley, New York, 1988).